Paper 50

Integrated Modelling of Geophysical and Petrophysical Data for Imaging Deeper Crustal Structures in Northern Sweden

Bastani, M. [1], Antal Lundin, I. [1], Wang S. [2], Jönberger, J. [1]

1. Geological Survey of Sweden, Department of Mineral Resources, PO Box 670, SE-751 28 Uppsala, Sweden
2. Uppsala University, Department of Earth Sciences, Villavägen 16, SE-752 36 Uppsala, Sweden

ABSTRACT

The Geological Survey of Sweden (SGU) conducted geophysical measurements and intensive geological studies in an area between city of Kiruna and Vittangi village in northern Norrbotten, Sweden. The main objective of study was to improve knowledge of the geology using modern methods, thereby creating supporting material for the exploration and mining industry in the region. In the summer of 2012 a 74-km-long reflection seismic profile was acquired between Kiruna and Vittangi for imaging bedrock contacts and the geometry of structures at depth. In 2014 the seismic profile was followed up with magnetotelluric (MT) measurements aimed at modelling the variation in electrical resistivity of the upper crustal structures. In this study we present models from the 3D inversions of MT, magnetic and gravity field data. We compare the results with those from the reflection seismic data to reveal some of the details of the physical properties, the geometry of upper crustal structures and the bedrock in the study area. The analysis of the models to a depth of 5 km along five selected sections demonstrates a reasonable correlation between the modelled physical properties, although some differences are observed. The reflection seismic and susceptibility models have better resolution in imaging shallower structures such as folds and smaller-scale structures, due to denser data sampling and higher sensitivity. However, the deeper structures (>2 km) seen in the reflection seismic image correlate better with the density and resistivity models. Towards the eastern part of the area very low-electrical resistivity structures seen in the resistivity model coincide with a zone dominated by sulphide and graphite mineralization. We propose a more detailed ground and airborne survey to identify potential areas for exploration.

INTRODUCTION

Over the past few decades 2D and 3D modelling of geophysical data such as gravity, magnetic, reflection seismic and electromagnetic data have played a key role in imaging crustal structures as deep as tens of kilometres (Li and Oldenburg, 1998; Pilkington, 1997; Portniaguine and Zhdanow, 2002; Zhdanov et al., 2012; England and Ebbing, 2012; Arora et al., 2012; Hedin et al., 2014; Cherevatova et al., 2015; Kamm et al., 2015). The geophysical models are generated by either forward or inverse techniques. Forward modelling uses *a priori* knowledge of the physical properties of the bedrock in the study area, for example, in the case of the gravity field, density. The *a priori* knowledge is usually gained from laboratory measurements on the physical properties of rock samples or, in some cases, known values extracted from other surveys with similar geological settings. On the contrary the inversion techniques are data-driven and the best model is achieved when the fit to data reaches a desired value.

In this study we present the results from 3D modelling of gravity, magnetic and electromagnetic data collected by the Geological Survey of Sweden (SGU) in the vicinity of the town of Kiruna in northern Norrbotten County in Sweden. Existing data in SGU's databases were compiled and mapped using GIS tools. These include ground gravity, airborne and ground magnetics, very low frequency (VLF), natural gamma radiation, petrophysical and ground geological observation data. The data in the study area were then extracted and imported into geophysical software for further analyses. At several locations ground geophysical measurements were carried out to fill in gaps in the existing data. New geophysical data, such as seismic reflection and magnetotelluric (MT) data with reasonably great penetration depth (> 5 km), were also obtained. The geophysical data were then processed and modelled in 2D and 3D using finite difference based inversions.

One objective of this study is to gain a more detailed understanding of the depth extent of known geological units and structures. The reflection seismic data collected by SGU along a 74-km-long profile (Juhojuntti et al. 2014) is used to check the validity of the models. We also show detailed comparisons between the forward modelling of ground magnetic field measurements and 2D inversion of ground VLF data with the existing borehole data along a 2-km long profile where graphite mineralization is identified.

GEOLOGICAL SETTINGS

The bedrock (Figure 1a) represents part of the Svecokarlian orogen, formed 1.9–1.8 Ga ago, and includes Archaean and early Palaeoproterozoic rocks. The Råstojaure complex, north of Kiruna, consists of meta-granitoids and subordinate meta-supracrustal rocks formed, deformed and metamorphosed in the Archaean.

In "Proceedings of Exploration 17: Sixth Decennial International Conference on Mineral Exploration" edited by V. Tschirhart and M.D. Thomas, 2017, p. 701–714

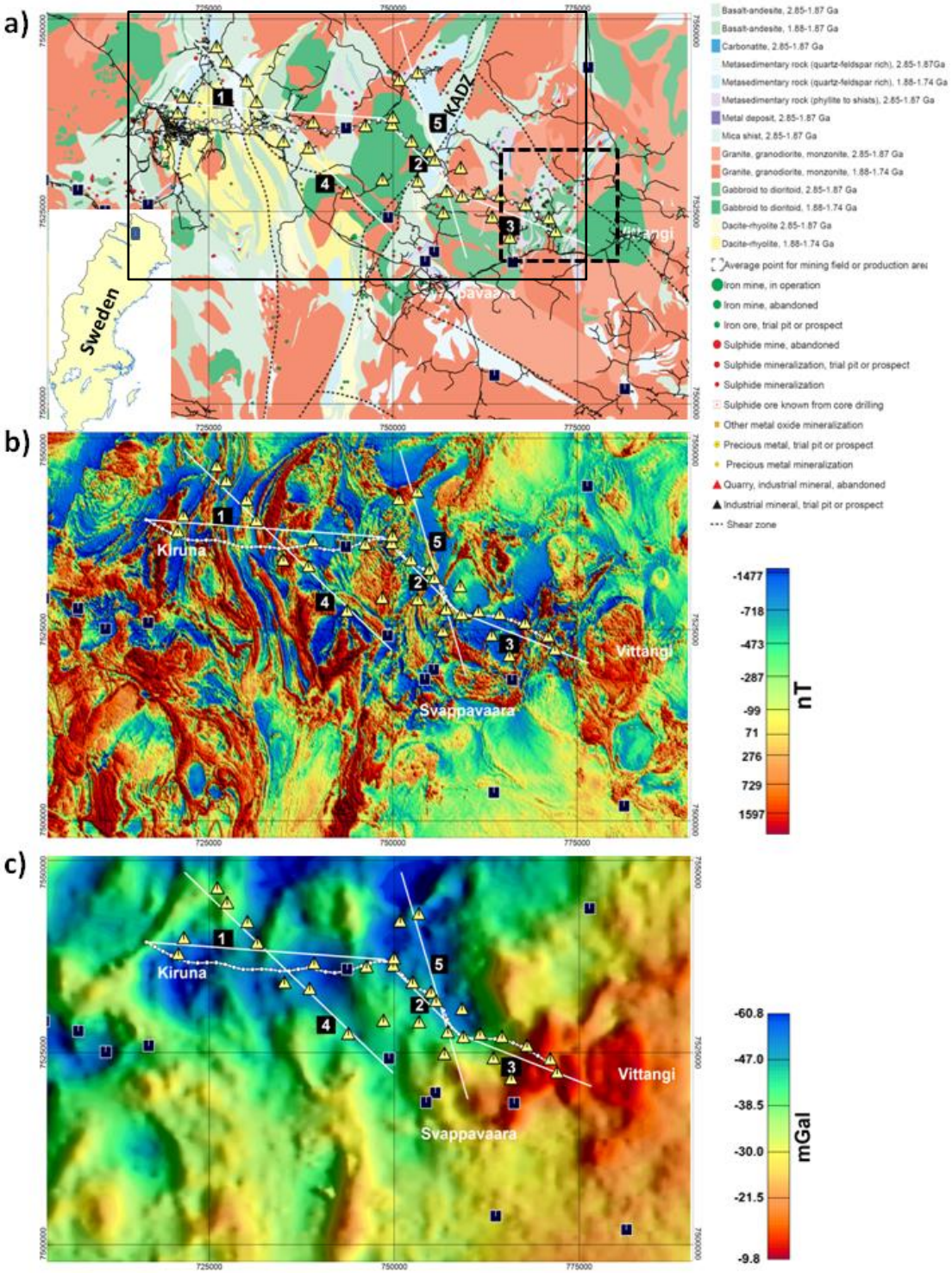

Figure 1: a) Simplified regional bedrock map of the study area (after Bergman et al. 2000). Area A shown by black rectangle. b) Map of total magnetic field anomaly. c) Bouguer anomaly map from ground measurements. The legends to the right in a) show the bedrock and mineralization in the area. The seismic reflection line is shown as a white line with white circles. The yellow triangles and the black squares are MT stations measured by SGU and Oulu University, respectively (see Bastani et al. 2015). The white lines with black squares (numbered in white) are the selected directions to show model sections from the 3D models (see Figure 2d). The dashed black rectangle marks the area chosen for detailed comparison between geophysical models, geological observations and the existing borehole data.

These rocks are unconformably overlain by meta-conglomerate, quartzite and meta-andesite-meta-basalt of the 12-km-thick Kovo group (Martinsson, 1999). The overlying Kiruna greenstone group (Martinsson, 1997) is estimated to be 14 km thick, consisting mainly of meta-basalt with lesser amounts of meta-ultramafic rocks, graphite schist, iron formation and marble. This unit hosts the Viscaria copper deposit as well as a number of occurrences of iron mineralization. Mafic dyke swarms cut the Råstojaure complex, and mafic sills are common in the Kovo and Kiruna greenstone groups. The Svecofennian supracrustal rocks and several suites of intrusive rocks were formed during the Svecokarelian orogeny. The Svecofennian supracrustal rocks unconformably overlie the Kiruna greenstone group, and consist of acidic, intermediate and basic meta-volcanic, and clastic meta-sedimentary rocks with a total thickness greater than 3 km. Kiirunavaara iron ore and several other iron deposits occur within these meta-volcanic rocks.

The youngest Svecofennian supracrustal rock in the area is a quartz-rich meta-sandstone (Hauki quartzite). Except for the youngest intrusive suite (Lina granite), all rocks in the area were affected by ductile deformation, hydrothermal alteration and greenschist to amphibolite facies metamorphism during the Svecokarelian orogeny.

Nd isotopic studies have shown that Archaean rock is probably present in the subsurface north of a line between Luleå and Jokkmokk (Öhlander et al. 1993). It is therefore highly probable that Archaean rocks can be found at depth in the Kiruna area. The outcrop pattern suggests that the general dip of the units is to the south (Juhojuntti et al. 2014). During ductile deformation large folds with wavelengths of up to several kilometres were formed, with steep axial planes and south-plunging fold axes. In the eastern part of the area the structure is more complicated, with several folding phases in different orientations. Foliations developed with strongly variable intensity. Ductile shear zones separate more weakly deformed domains. The two most important shear zones are the Karesuando–Arjeplog deformation zone (KADZ) in the east and the Kiruna–Naimakka deformation zone in the west (Bergman et al. 2001), with widths of 8-10 km, including less deformed lenses. Ductile shear zones are commonly reactivated in the brittle regime. Some copper and gold mineralization can be found along the KADZ.

At the eastern end of the seismic profile (Figure 1a) the Vittangi greenstone group (VGG), which forms the central part of the Nunasvaara key area, contains 61 mineral deposits, prospects or showings (Lynch and Jönberger 2013), the main commodity being graphite-bearing schists (e.g. Nunasvaara).

GEOPHYSICAL DATA

SGU conducted airborne geophysical measurements during 1960–1964 in the study area. The magnetic field was measured as a part of the iron inventory programme Loussavaara-Kiirunavaara AB (LKAB) collected denser airborne data during 1979–1984 in the same area. LKAB carried out airborne magnetic field, electromagnetic (both VLF and Slingram) and gamma ray radiation data acquisition. The survey direction was east-west. All airborne surveys in the area were made with a line separation of 200 m, a point distance of 40 m and a nominal ground clearance of 30 m. The magnetic anomaly map (Figure 1b) of the same area (shown in Figure 1a) has complicated patterns, such as banded, folded and circular features that are caused by supracrustal and intrusive rocks. The data contain valuable information that can be used to study the deformation history of the rocks.

Regional gravity measurements were made by SGU and the Swedish Mapping, Cadastral and Land Registration Authority (LMV) during different periods, most intensively between 1960 and 1985. The distance between the measurement points varies between 300 and 3000 metres. Gravity data (Figure 1c) are shown in the form of Bouguer anomaly maps. The gravity highs can usually be related to mafic magmatic rocks at depth. Gravity lows coincide with the distribution of supracrustal rocks with felsic compositions. In summer 2012 a seismic reflection profile approximately 74 km long was acquired by SGU in the Kiruna area (shown by white circles in Figures 1a to 1c). The main aim of the seismic measurements was to better understand the upper crustal structure in the Kiruna area, e.g. by imaging bedrock contacts and deformation zones. The western end of the seismic profile is only a few kilometres from the Kirunavaara mine, and close to the profile are several known zones of mineralization, some of which are active exploration targets. For more details of the data acquisition parameters the reader is referred to the report by Juhojuntti et al. (2014).

Magnetotelluric measurements were conducted in two areas (A and B in Bastani et al. 2015) in northern Norrbotten during the summer of 2014 (Figures 1a to 1c). The survey objectives were to model the variation of electrical resistivity of the upper crustal structures along the reflection seismic profile collected in the summer of 2012 (Juhojuntti et al. 2014) and to study the depth extent of known mineralization. The collected MT signals cover a wide frequency band, from 10^{-2} to 300 Hz. 2D and 3D modelling of the collected data images the variation of electrical resistivity down to depths > 30 km. Bastani et al. (2015) give a detailed account of the results from 2D modelling of collected MT data along two selected directions in two areas. Here we show the results from the 3D modelling of MT data in area A. At the eastern parts of the study area close to the Vittangi village (see Figure 1 for location) ground magnetic field and VLF data collected by SGU were used to model shallower structures that enabled us to directly compare them with the existing borehole information in the area, down to depth of about 150 m.

MODELLING RESULLTS

We used the VOXI program for the 3D inversion of the potential field data. It is a 3D finite difference inversion module by Geosoft Inc. in the Oasis montaj software package. We tried several inversions using different parameter settings. Here we present models with the responses as close as possible to the field and laboratory observations and measurements. The resulting 3D models are shown as density contrasts and magnetic susceptibility in Figures 2a and 2b, respectively. The dimensions of model cells are 500 m × 500 m × 250 m in x, y and z directions, respectively. We used petrophysical data and constrained model susceptibility within the range of 0.00001 to 2.0 SI units with a background susceptibility of 0.0 SI. The unusually high-upper susceptibility limit of 2 SI was imposed to

enable the inversion to take into account the several known iron ores in the area, of which the world-class Kiruna iron ore is best known. A background density of 2.70 g/cm^3 and density contrast of between -0.12 g/cm^3 and 0.9 g/cm^3 were used to constrain the density model.

We used the 3D inversion code WSINV3DMT by Siripunvaraporn et al. (2005) to carry out 3D modelling of the MT data using a smoothing regularization. The resulting 3D resistivity model is shown in Figure 2c. Note that the model is presented in the inversion's local coordinate system.

The susceptibility model (Figure 2b) contains higher frequency variations, which is mainly due to denser sampling and partly to the higher sensitivity of the method compared to gravity and MT. The MT data do not have sufficient resolution at the surface due to the low-frequency content of the signal.

Selected Susceptibility, Resistivity and Density Sections from 3D Models- A Regional Overview

It is not easy and straightforward to compare the models in 3D. Hence, five portions of the 3D models from single 3D inversions of various data sets numbered 1–5 (plotted on Figure 2a) were selected in the form of depth sections for more detailed comparison. The sections cross a few known geological structures and mineralised zones. The selected portions are shown on the density model in Figure 2a. For example, the density contrast depth sections (here called sections) from the 3D gravity model are shown in Figure 2d. Sections 1 to 3 are collocated with three portions of the seismic reflection profile (Figure 1) reported by Juhojuntti et al. (2014) are presented in this paper. Along each direction we present model sections showing susceptibility, resistivity and density contrast. In each resistivity section we superimposed the contours of the estimated susceptibilities and above each resistivity section part of the bedrock geology map along the same section is shown. The location and type of known mineralization is also shown to facilitate comparison and interpretation.

Comparison of the 3D models with the information in the seismic reflection data was rather difficult, mainly because of the weak reflection patterns seen in the seismic data. In a separate section we compare the seismic images with the 3D models, where a clear reflection pattern could be extracted to interpret regional structures in a more integrated manner. One should always bear in mind that the smoothing regularization used in all the 3D inversions generates models with considerably smooth transition zones that might not match sharp geological boundaries.

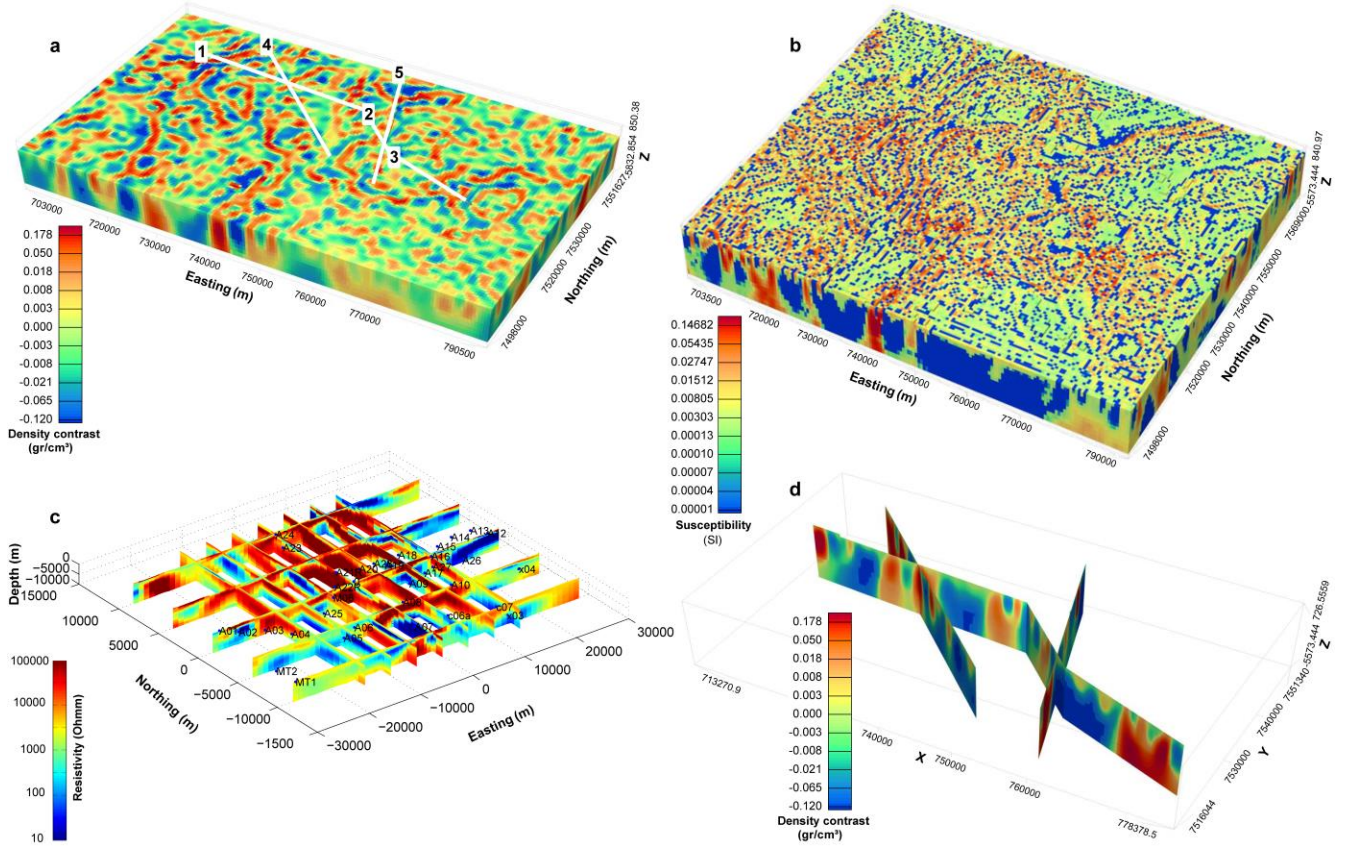

Figure 2: a) 3D density contrast model from the inversion of Bouguer anomaly data in the area. The selected section lines are shown in white. b) The 3D susceptibility model from the inversion of magnetic field anomaly data shown in Figure 1b. c) Resistivity model from the 3D inversion of MT data. d) Density contrast sections taken from the model shown in a) along the selected sections (see Figure 1).

Section 1

This section is 32 km long and runs approximately west-east. Although distribution of the MT stations is sparse along section 1 (see Figure 1) the 3D inversion model reveals valuable information along this section (Figure 3). To make the comparison easier the modelled physical properties of various geological structures and units mapped along each section are summarised in Table 1.

Structure/unit	Magnetic susceptibility ($\times 10^{-5}$ SI)	Resistivity (Ohm m)	Density contrast (g/cm^3)
Sedimentary rocks	Low (<100)	Low (< 1000)	Low-intermediate (-0.07–0.00)
Felsic volcanic rocks	Low	Intermediate (1000–4000)	Low (<-0.07)
Mafic volcanic rocks	High (>5000)	Not resolved	High (>0.06)
Shear zones	Low	Low	Low
Granitoids	Low-intermediate	High (> 4000)	Low
Mafic intrusions	High	Very high (> 10000)	High (>0.06)

Table 1: Summary of the estimated physical properties of various geological units and structures along section 1

The susceptibility model shows more details and resolves structures resembling major folds with varying dips that contain minor/smaller folds (higher frequency near surface susceptibility variations). The white and black arrows indicate the apparent average dips of major high- and low-magnetic susceptibility structures, respectively. The arrows are also shown on the resistivity and density contrast sections. For example, a few zones with susceptibilities > 0.05 (5000×10^{-5} SI units) dip almost vertically in the mid-western part of the section. An easterly-dipping structure in the western part of the model and a steeply east-dipping structure in the middle of the model (close to 730000 E) demonstrate variations in the dips of the modelled susceptibilities/structures, indicating possible presence of folded structures. The western to the central part of the resistivity model is dominated by a low-resistivity zone with very faint high-resistivity structures. However, the lowest resistivity zones correlate very well with the lowest susceptibility zones (shown by black arrows) that reach very close to the surface. A good example coincides with a mapped shear zone in the middle part of the model. Towards the western end of section 1 Juhojuntti et al. (2014) reported an east-dipping structure in the seismic data at CDP 500, which may be associated with Hauki quartzite, which forms the eastern contact of the east-dipping high-susceptibility structure. This dip is not observed in the resistivity model, but corresponds with a low-density zone in the density model. It should be noted that dips from the high-magnetic structures (white arrows) shown on the density model are reasonably collocated with the high-density zones. The resistivity and density contrast models seem to have a better depth penetration and contain structures at depths > 2.5 km that are not resolved in the susceptibility model. The west-dipping low resistivity and low-intermediate density zone at the western end of the section (west of 740000 E) and the low-density and high-resistivity features (Figs. 3b and 3c) to the east of this structure (east of 720000 E) are two examples. The high-resistivity structure at depths below 3000 m, east of 720000 E, may be caused by intrusive rocks which, due to the negative density contrasts, are probably felsic intrusions.

Sections 2 and 3

Figure 4 shows the models along sections 2 and 3. The MT data along the ~15-km-long section 2 has better coverage than section 1. Table 2 shows the modelled physical properties of geological units and structures along sections 2 and 3.

Structure/unit	Magnetic susceptibility ($\times 10^{-5}$ SI)	Resistivity (Ohm m)	Density contrast (g/cm^3)
Sedimentary rocks	Low (<100)	Low (< 1000)	Intermediate (0.00–0.02)
Felsic volcanic rocks	Low	Not resolved	Low (<-0.07)
Mafic volcanic rocks	High (>5000)	Intermediate (1000–4000)	High (>0.06)
Karesuando–Arjeplog deformation zone (KADZ)	Low	Low	Low
Granitoids	Low-intermediate	Intermediate (1000–4000)	Low-intermediate (-0.07–0.01)
Mafic intrusions	High	Intermediate–high	High (>0.06)

Table 2: Summary of the estimated physical properties of various geological units and structures along sections 2 and 3.

Extremely high-resistivity (> 20000 Ohm m) and relatively high-susceptibility and high-density zones are resolved (west of 756000 E) along section 2 (Figures 3a–c). The high-resistivity zone continues down to a depth of ~4 km with a northwest-dipping trend. The same dip is observed in the susceptibility and density models. However, the magnetic model estimates a maximum depth of 3 km, and the density model a depth of approximately 3.5 km. On the geological map the first 4 km of the section in the west is marked as a gabbro intrusion with inclusions of granitoid. At the point of granitoid inclusion modelled resistivity decreases towards the west, and susceptibility shows some slight changes. The density model indicates low values in this interval that do not match the geological information and indicate intrusions of a more felsic nature. Towards the east of the KADZ the resistivity and density models show a dramatic change, with decreasing values, especially at deeper levels (resistivities < 500 Ohm m and density contrasts < -0.12 g/cm^3). Close to this contact a few occurrences of sulphide mineralization are reported in SGU's mineral resource database. A folded-form structure can be seen on the magnetic anomaly map along this section (Figure 1b) and modelled susceptibility also suggests a folded structure in the form of a syncline that continues to a depth of ~2 km. It is obvious that the folded structure within the KADZ is more like an anticline fold (see Figure 1a for location), with a northwest-

dipping, high-susceptibility structure most likely caused by highly magnetic volcanic rocks.

Section 3 is 19 km long and has a westnorthwest-eastsoutheast orientation. A high-susceptibility structure dipping northwest shows up at the westnorthwest end of the section. Further east, the section crosses granitic rocks with low-susceptibility contrasts. Occurrence of low-density, quartz monzodioritic rocks at the eastern gradient of the gravity low was mapped by Lynch and Jönberger (2013). Our data suggest that the intrusive rocks here are predominantly of felsic composition at depth, which is confirmed by the forward modelling presented by Juhojuntti et al. (2014). At coordinates SWEREF99 TM 767971/7523890 the section cuts the Nunasvaara area with known graphite, iron and sulphide mineralization, hosted by VGG rocks. The group is dominated by volcanic, volcanoclastic and sedimentary rocks, and cut by doleritic sills (Lynch and Jönberger 2013). The susceptibility model suggests steeply dipping, folded structures that deepen to the southeast. There is good correlation with the 2D interpretation of the gravity and magnetic data made by Juhojuntti et al. (2014). The resistivity section is mainly dominated by a very low-resistivity feature east of KADZ. Resistivity decreases considerably with depth, reaching values < 500 Ohm m. Based on various reports (e.g. Lynch and Jönbeger, 2013; Martinsson, 2011 and references therein), this area is dominated by graphite and sulphide mineralization and, in the most easterly part, is best known for schist-hosted graphite deposits (e.g. Nunasvaara), which represent the largest known graphite resource in Sweden. The susceptibility model also indicates the presence of an extremely low-susceptibility zone at a depth > 2 km. The density section depicts a huge contrast in the middle part in which a very high-density zone continues to depths > 5 km is resolved in the eastern part of the section. Shallower density variations indicate folded structures with dips that correlate well with those predicted by the susceptibility model. High densities and high susceptibilities may be directly related to the mafic volcanic rocks and intrusions mapped in the area. The very low-density zone at depth in the western part of the density model may be caused by a granitic intrusion observed in the area. Two scenarios are suggested for the deep and very low-resistivity feature that starts at 756000E and

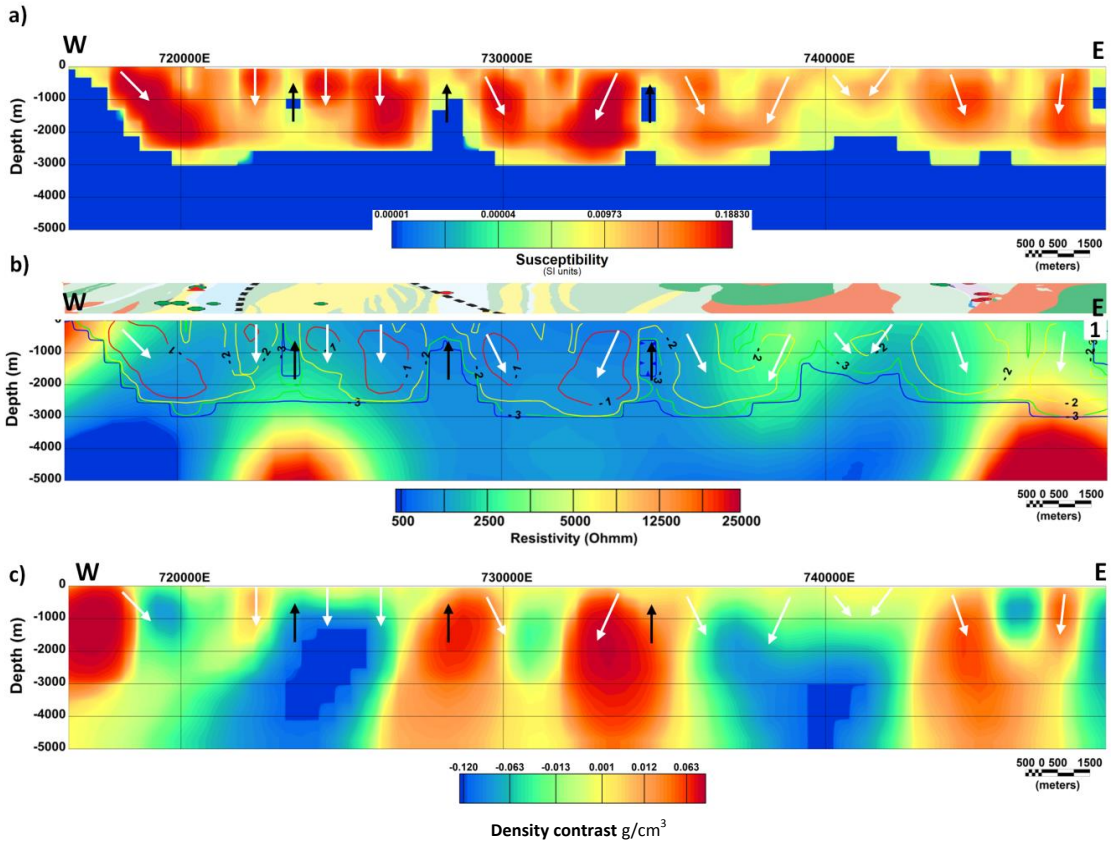

Figure 3: Sections from 3D models along section 1 plotted in Figures 1 and 2. a) Susceptibility, b) Resistivity, c) Density contrast. In b) the resistivity model is in the background and the contours with different colours represent the estimated magnetic susceptibility in logarithmic scale. The mapped bedrock and known mineralization along each direction are shown on top of the resistivity section. The white and black arrows indicate the interpreted dips of high- and low-susceptibility zones, respectively.

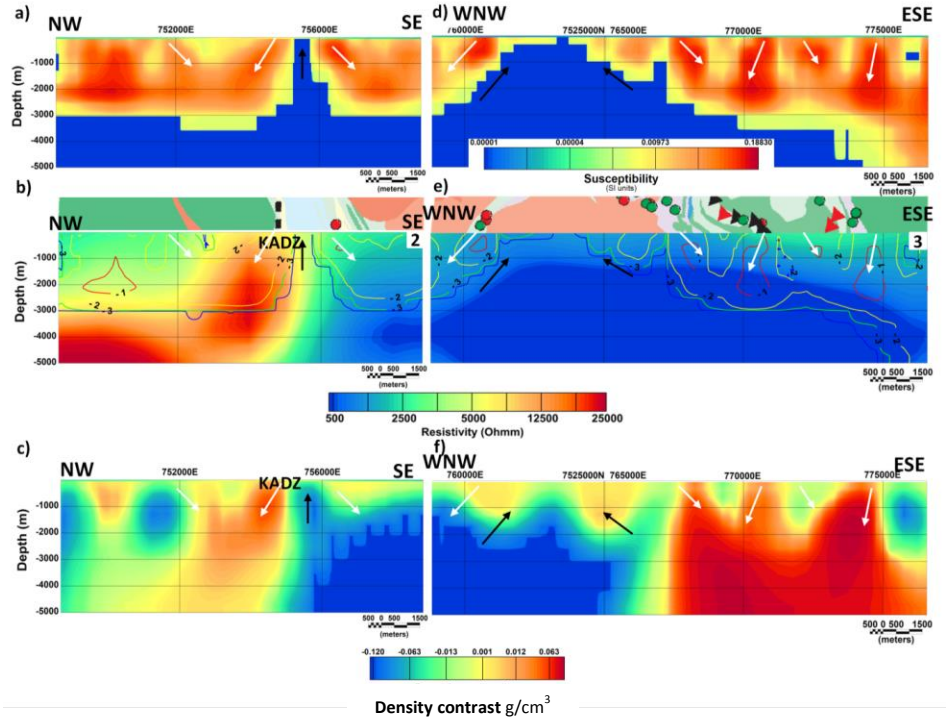

Figure 4: Sections from 3D models along sections 2 and 3 plotted in Figures 1 and 2. a) Susceptibility, c) Resistivity, c) Density contrast along direction 2. d) susceptibility, e) resistivity, f) density contrast along direction 3. In b) and e) the resistivity model is in the background and the contours with different colours represent the estimated magnetic susceptibility in logarithmic scale. The mapped bedrock and known mineralisations along each direction are shown on top of the resistivity section. The white and black arrows indicate the interpreted dips of high and low-susceptibility zones, respectively.

continues to the end of section 3: a) the highly conductive mineralizations observed in the area (Martinsson 1993) or b) a deep-seated rock type with low resistivity, susceptibility and density. The latter is considered more likely due to the geometry and extent, although the extremely low resistivity is hard to explain. This is a scientific question to be answered by future research.

Comparison with Seismic Reflection Sections

We compare the models shown along sections 1, 2, and 3 with the migrated seismic reflection sections reported by Juhojuntti et al. (2014). Along sections 1 and 3 we compare the susceptibility and density contrast models, whereas along section 2 the resistivity model is also included. The comparison is mainly qualitative because much more detail is seen in the seismic sections due to the higher data sampling density. We show the seismic section on top of the selected models and use arrows and broken lines to indicate the most dominant reflection patterns, i.e. the stronger reflections that are clearer in the seismic sections. Figure 5 shows seismic section 1. The broken black line marks the bottom of shallower reflections above a depth of approximately 1 km, where the reflectivity is substantially higher. The smaller arrows show the apparent dip of dominant reflections. In the depth range 0–1 km, the apparent dip of shallower reflections agrees reasonably well with those seen in the susceptibility and density contrast models. However, dips are gentler in the seismic section (compare with those shown in Figures 3a and 3c). Below 2 km, the susceptibility model does not resolve any contrast and the best comparisons can be made between the density contrast model and the seismic reflection sections. Generally speaking, below this depth the reflections are weaker and sparser. In the west, an almost horizontal high-reflectivity zone predominates at depths > 4 km, while to the east, after 720000 E, a 45° west-dipping high-reflectivity zone clearly dominates until 730000 E. These higher-reflectivity zones coincide very well with the low- and high-density zones with approximately the same dips. Further east, the dominant dip of the high-reflectivity zone at depth changes is reversed and coincides with a high-density zone (Figure 5b). We have marked two deeper reflectivity zones with "?" that seem to be artefacts caused by the migration process. The down-dipping reflection trend is dominant towards the eastern end of the section and no significant correlation can be seen with either the susceptibility or the density contrast models.

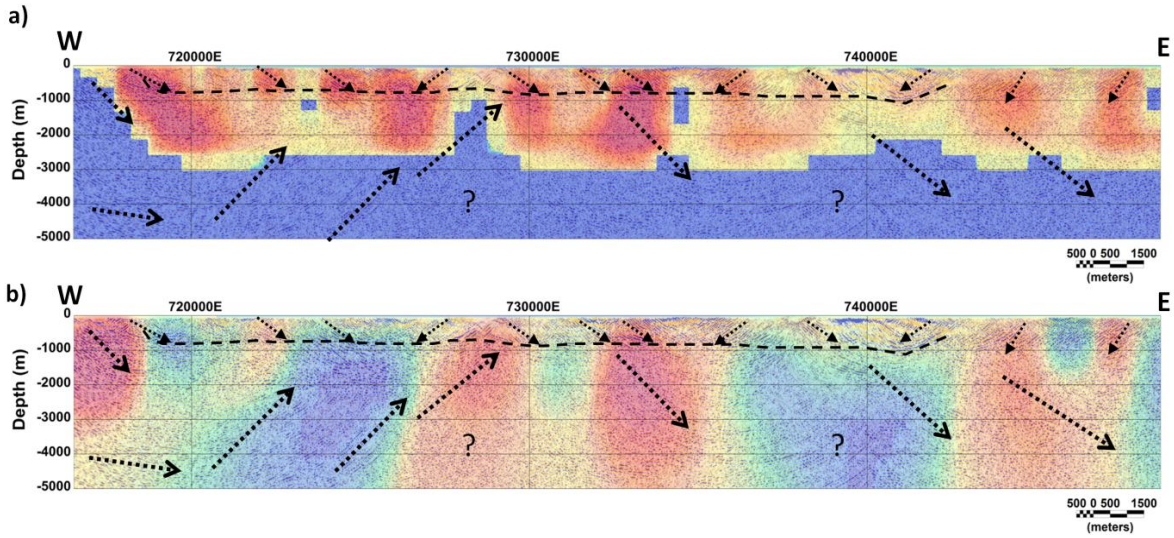

Figure 5: Comparison between the migrated seismic section with a) the susceptibility model and b) the density contrast model along section 1. The smaller arrows indicate shallower and more local predominant trends. The longer arrows represent deeper reflections. The broken black line marks the bottom of a shallower high-reflectivity zone in the seismic section. The "?" shows possible artefacts caused by migration.

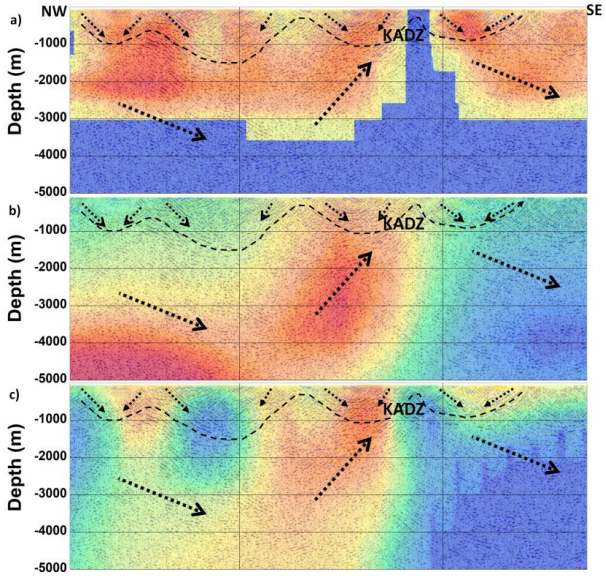

Figure 6: Comparison between the migrated seismic section with a) susceptibility model, b) resistivity model and c) density contrast model along section 2. The smaller arrows indicate shallower and more local predominant trends. The longer arrows represent deeper reflections. The broken black line marks the bottom of a shallower high-reflectivity zone in the seismic section.

Figures 6a to 6c show the comparison between susceptibility, resistivity, density contrast models and the reflection seismic data along section 2. The apparent dips of shallower reflections (marked by smaller arrows) correlate well with the highs and lows seen in the susceptibility model (Figure 6a) and to some extent with the structures seen in the density contrast model (Figure 6c). In the 1–3 km depth range, the first third of the section in the northwest, a moderately southeast-dipping high-reflectivity trend (marked by a long arrow) predominates in the seismic section and coincides best with the high-susceptibility zone. Further southeast the dip changes to the northwest, which can be interpreted as a regional synclinal structure. Northwest-dipping strong positive susceptibility, positive density contrast and a high-resistivity zone are clearly observed in this part of the sections (Figures 6a to 6c). With the exception of a few shallow diffractions in the seismic section, the KADZ is not resolved as clearly as in the other sections. Towards the southeast of the KADZ the regional dip trend in the seismic section reverts towards the southeast. It should be noted that at the deeper levels in this part of the section (> 3 km) fringe-shape reflection may have been introduced by the migration processes.

The seismic data cover the first two-thirds of section 3 (Figure 7). The apparent dip of shallower reflections is dominated by eastsoutheast and westnorthwest trends in the first and second half of the section, respectively. The deeper reflections show varying dips in the first half of the section, whereas the second half is dominated by a westnorthwest-dipping high-reflectivity zone that starts at the position where an almost vertical high-density zone appears in the density model. High-density mafic volcanic and gabbro intrusions are mapped at this boundary. Two very distinct almost horizontal reflectors, marked by a long horizontal arrow at a depth of 2.5–3.5 km, are of great importance in the seismic section. These were interpreted as smaller mafic bodies in the forward model presented by Juhojuntti et al. (2014). Neither the magnetic nor the gravity inversion model reveals such a distinct zone, although a weak gradient in the density contrast model can be distinguished in that area.

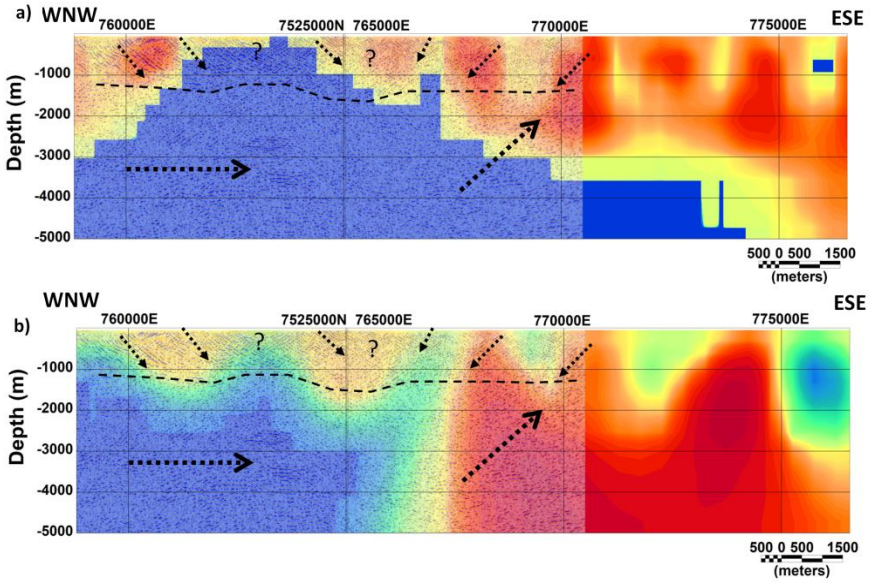

Figure 7: Comparison between the migrated seismic section with a) susceptibility model and b) density contrast model along section 3. The smaller arrows indicate shallower and more local predominant trends. The longer arrows represent deeper reflections. The broken black line marks the bottom of a shallower high-reflectivity zone in the seismic section. The "?" shows possible artefacts caused by migration.

2D Modelling and Detailed Comparison with Petrophysical and Borehole Data

The area marked by the dashed black rectangle in Figure 1a was selected to show a detailed comparison between the geophysical models and existing geological and borehole information. The bedrock in the Nunasvaara area (selected area) is dominated by meta-volcanic and meta-volcaniclastic rocks of basaltic to andesitic composition, meta-sedimentary rocks including graphite-bearing black schist, and meta-dolerites (Figure 8a). These rocks are part of the VGG, which is of approximately 9 km × 11 km extending in northnortheast direction (Eriksson and Hallgren, 1975). The VGG in this area is surrounded by intrusions ranging from gabbro to granite belonging to the Haparanda, Perthite monzonite, and Lina suites. Several mineralization occurrences are found, including skarn-iron and graphite deposits. In Figures 8b and 8c we show two examples of geological sections from interpretation made by Gerdin et al. (1980) based on the existing boreholes at three locations (B1, B2 and B3). They report frequent occurrences of nearly vertical graphitic horizons with varying thicknesses. For a more detailed description of the geology and lithostratigraphy around Nunasvaara, the reader is referred to the report by Lynch and Jönberger (2013).

A considerable amount of airborne geophysical information is available for the Nunasvaara area. In addition, dense ground magnetic, slingram and gravity measurements have been taken over the entire area, together with extensive sampling for petrophysical analysis (yellow symbols on the magnetic field map in Figure 9a). More information regarding these previous geophysical investigations can be found in Lynch and Jönberger (2013).

The overall pattern seen on the magnetic field data (Figure 9a) represents the lithological units in the area. The bedrock mainly consists of basaltic to andesitic meta-volcanic rocks (tuffs) and meta-dolerites. The magnetic properties vary considerably which is clearly reflected in the diagram shown in Figure 9b. These variations can be seen on the magnetic anomaly map in the western part of the area where the tuffs generate both a banded pattern of relatively narrow, high magnetic anomalies along with areas of considerably lower magnetic signature. Sequences of skarn iron ores, mainly in the western part of the area, cause the strongest anomalies in the magnetic map. The ground magnetic data also show the various folding events that the area has been subjected to. The high densities of the meta-volcanic rocks and meta-dolerites (averaging 2.958 g/cm^3 and 2.979 g/cm^3, respectively) give rise to a dominant gravity high in the area (Figure 1c).

Forward modelling of the gravity and magnetic field data was carried out using the Potent software from Geophysical Software Solutions. The background density and susceptibility have been set to 2.70 g/cm^3 and 100 × 10^{-5} SI, respectively.

In this paper we show the modelling results along Profile 1. This is an area where the different lithologies of the greenstones are tightly pinched between intrusive rocks on either side. The ground VLF data were also acquired along the same profile, the extent of which crosses several black schist horizons. The results of the modelling are displayed in Figure 9c, clearly showing the greenstones between the intrusions on either side. In order to achieve a better understanding of the depth extent of the intrusions, the profile was extended during the modelling stage both to the northwest and southeast to make use of the regional gravity field data.

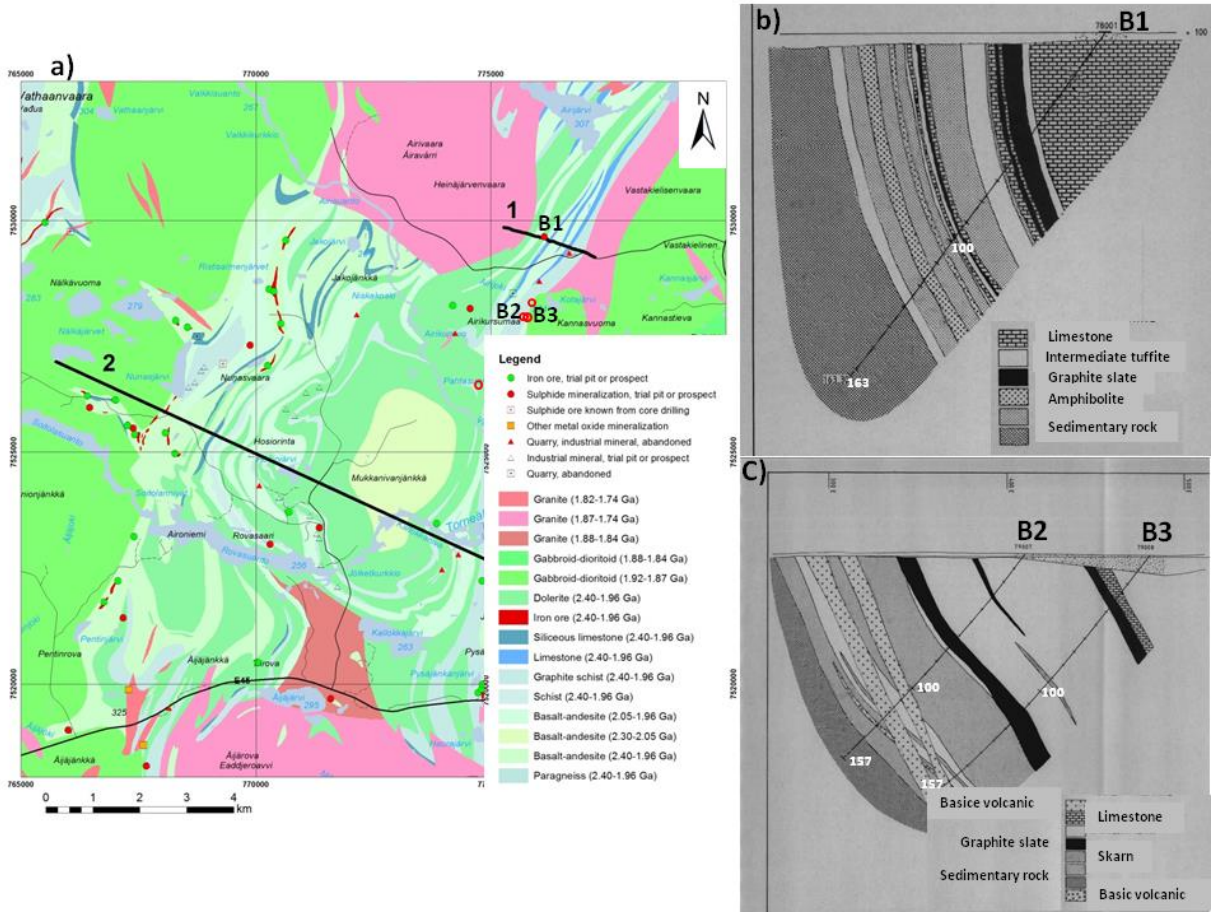

Figure 8: a) Bedrock map in the area around Nunasvaara (after Bergman et al. 2012). The mineralization occurrences are posted on the map and described in the legend to the lower right. Black lines with numbers (1 and 2) represent the extent of profiles which have been modelled using geophysical data. b) Geological interpretation/section based on observations in borehole B1. c) Geological interpretation/section based on the observations in boreholes B2 and B3. Locations of boreholes are shown in a) with red circles and are marked text B1–B3. The figures in b) and c) are modified from a prospecting report by Gerdin et al. (1980). The numbers with white text in b) and c) represent depth in the boreholes.

The profile is located across a gravity high, which strikes in a southwest-northeast direction and coincides relatively well with the basic volcanic rocks and meta-dolerites. The northwestern and southeastern part of the profile lies within granite intrusions with an average density of 2.62 g/cm^3. In Figure 9c on the geological model we show variation of the magnetic susceptibility and the average density of each geological unit. It should be mentioned that posted susceptibility values on each geological unit illustrate the range of variations of the susceptibility within the entire study area. This means that for the same geological unit along the profile different susceptibilities in that range are used to get a proper fit to the data. For example the susceptibility used for the granite in the model is 100×10^{-5} SI. The model shows that the granite intrusion in the west continues under the greenstones which deepen towards the east down to 800 m below ground level in the central and eastern part of the sequence. The maximum gravity anomaly along the profile is however reached in the eastern part, close to the contact with the granite intrusion. In order to compensate for this, a body with mafic properties has been added to the model (dark green body in Figure 9c), underlying the granite.

In Figure 9c, above the susceptibility model, resistivity model from 2D inversion of VLF data is presented with the same scale. For the inversion we have used REBOCC program (Siripunvaraporn and Egbert, 2000). The resistivity model is shown down to 250 m where the limit of depth penetration of the VLF signal is reached. A relatively conductive segment is illustrated in the resistivity model between 400–1200 m. According to the densely sampled ground slingram measurement (not shown here), geological observations and borehole data (see Figures 8b and 8c) this part of the profile is located in an area with several closely spaced conductive horizons. The grey bodies on the susceptibility model represent black schist horizons that contain considerable amounts of graphite. These bodies have been adopted from the interpretation of the VLF profile. Several strong conductive features appear close to the surface in the resistivity model. Starting from the west a narrow conductive feature is located 350 m from the western end of the profile. The dip of this

feature is steep towards the east and has a depth extent of approximately 100 m. This is likely the westernmost horizon of the black schist, situated at the contact between the granite intrusion and the greenstones. Continuing further east, additional conductive, vertical horizons are visible at distances 650 m, 1100 m and 1750 m along the profile. The one at 650 m is close to the location of borehole B1 shown in Figure 9b where a nearly vertical graphitic schist zone is interpreted in the geological section (Figure 8b). The depth extent of the graphitic zones in the resistivity model can be quite inaccurate because of limited depth penetration of the VLF signal. However their lateral extents are rather well-determined.

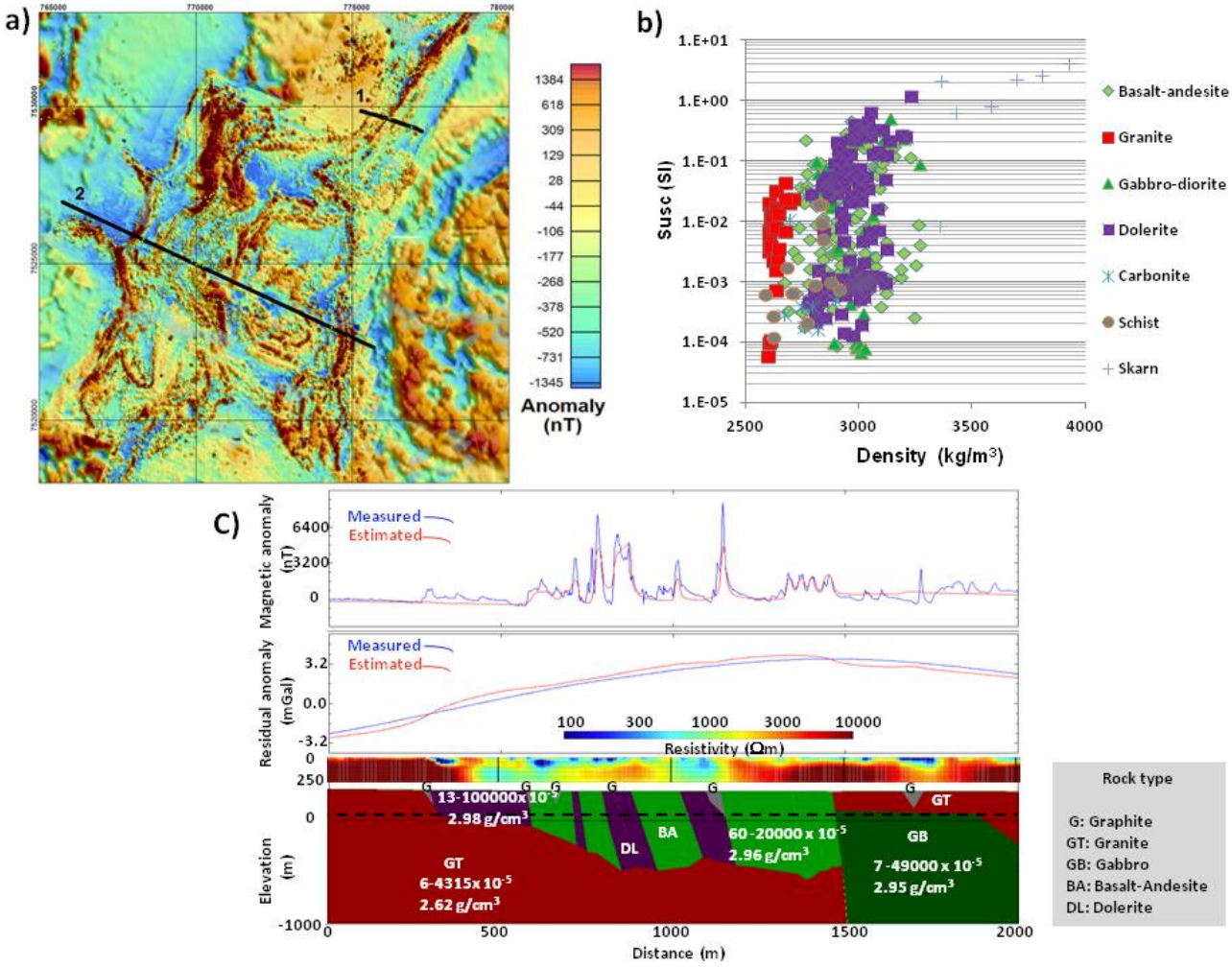

Figure 9: a) Map of the magnetic field anomaly in the area shown in Figure 8a. Location of petrophysical samples are posted on the map with yellow circles. Black lines with numbered 1 and 2 represent the extent of profiles which have been modelled using geophysical data. b) Variation of measured magnetic susceptibility of the rock samples versus measured densities in the lab. See the legend to the right for the rock types. c) Geological model from forward modelling of ground magnetic field and gravity data along profile 1 (bottom frame). The measured susceptibilities and densities of each geological unit are shown on the model with white numbers. The rock types are shown in the legend to the right of the model. The first frame above the susceptibility model is the resistivity model from 2D inversion of ground VLF data collected along the same profile. The dashed black line on the geological model marks the bottom of the resistivity model. The two other frames from bottom to top show the measured and estimated residual gravity and magnetic field data, respectively.

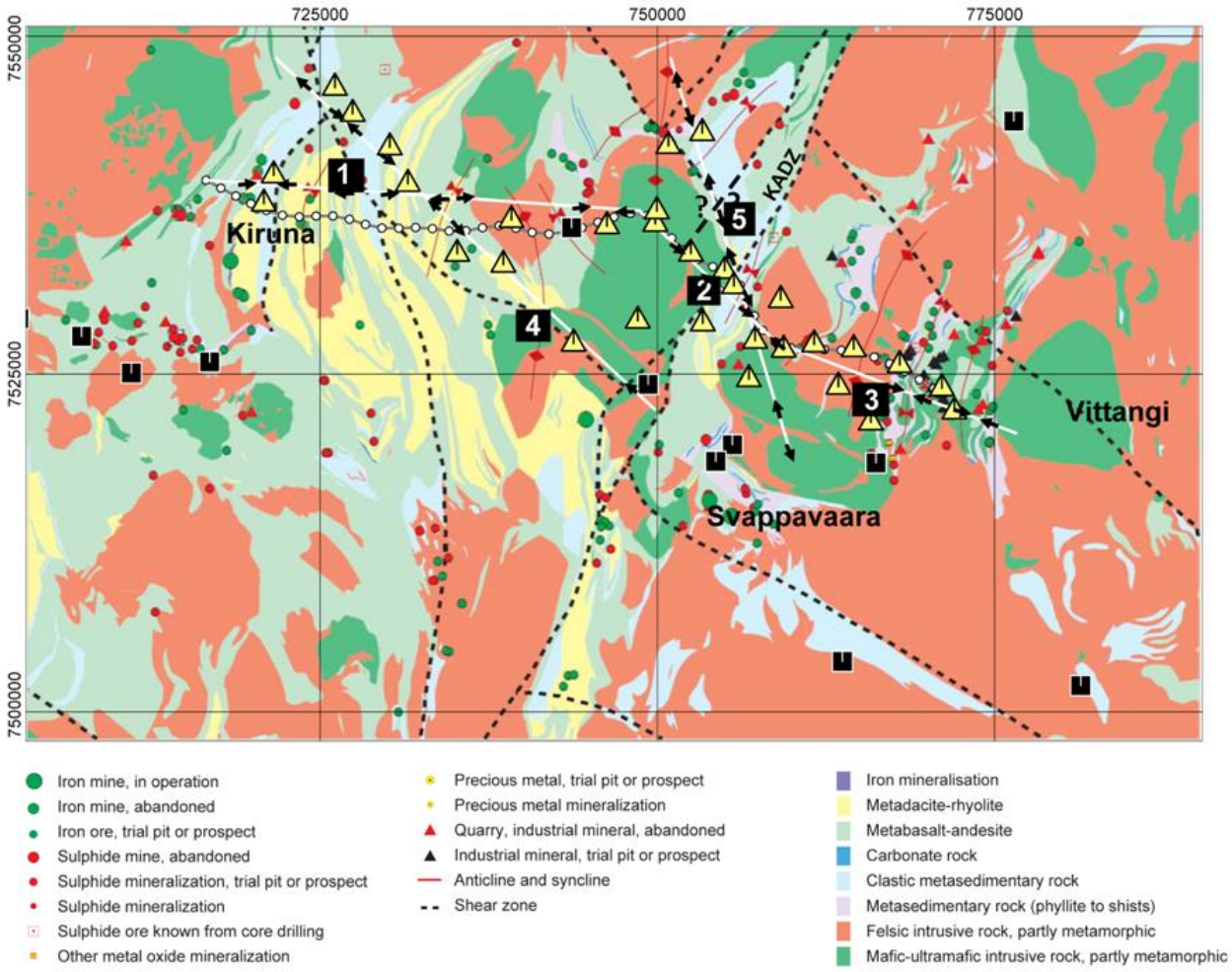

Figure 10: Regional presentation of the estimated dips of structures with moderate to high magnetic susceptibilities taken from the 3D inversion results shown on the bedrock geology map of the study area. Most of the dips are confirmed by the seismic reflection data. The interpreted fold structures from geological observations reported by Eriksson and Hallgren (1975) are also presented for comparison.

DISCUSSIONS

Figure 10 shows a more regional summary of the estimated apparent dips along sections 1 to 5 (note that in this paper section 1 to 3 are presented) taken from the magnetic susceptibility models and seismic sections (1–3) shown on the geological map in the area. The black arrows point towards the down-dip. Note that the dips are presented for moderate to high-susceptibility structures. In our interpretations we have also taken some account of the density and the resistivity models. A few arrows might represent the steeply dipping structures that are shown in the magnetic models with vertical arrows. The thicker broken line marked by a "?" indicates possible continuation of the shear zone mapped in the northeast and crossing section 5. This approach can be applied to the entire model area to construct a more detailed image of variation of the dip direction. To verify the validity of our dip interpretations we have compared them with an analysis made by Eriksson and Hallgren (1975). The folds (anticlines and synclines) interpreted by their study are shown in Figure 10 by red symbols. We generally find a good correlation between the geological structures presented by Eriksson and Hallgren (1975) and those derived independently by interpreting models from different geophysical responses. However, there are also some differences, giving us new information and insights. In the middle part of section 1, east of 730000 E, the susceptibility model suggests an anticline (Figure 3a). The same pattern is also observed in section 4 (not shown here), near the intersection with section 1, while the geological observations reported by Eriksson and Hallgren (1975) show a synclinal structure (Figure 10). This is also the case along the eastern part of KADZ (Figure 10) where sections 2 and 5 cross each other. The susceptibility and the density sections show an anticline (Figures 4a, 4c), whereas the geological model/interpretation shows a syncline (Figure 10). In this case, the seismic section also suggests an anticline structure at depth (Figure 8). It should be noted that the geological observations and geophysical models have somewhat different scales, which gives rise to different interpretations.

CONCLUSIONS

The models from 3D inversions of the potential field and the MT data demonstrate a reasonable correlation with mapped geological units and mineralized zones in the area. As expected, shear zones appear as low-resistivity, low-susceptibility and low-density zones in the selected sections from the 3D models. High-susceptibility and high-density zones mark the basaltic volcanic rocks and in most of the cases, appear as high-resistivity zones in the resistivity models. A very distinct low-resistivity and low-susceptibility zone of varying density (high and low) is observed in the eastern part of section 3, where zones of sulphide and graphite mineralization is known. The MT method has a poor resolution at shallower depths but a reasonably deep depth penetration. The 3D resistivity models can be used to study geometry and properties of deep-seated crustal structures as deep as 50 km. The VLF method demonstrated a good potential to detect and model shallow low-resistivity zones though it lacks enough penetration to model the depth extent of the conductive zones. The susceptibility 3D models, on the other hand, demonstrate a reasonably high-resolution near the surface and are best for comparison with the high-resolution seismic reflection data for the study of shallower structures and geological units. Dips estimated using the susceptibility models correspond fairly well with those from seismic data. However, the smoothing regularization used in the 3D modelling and the coarser sampling of the magnetic data led to big differences in some portions of the sections. The density, resistivity and seismic reflection data correlate best in deeper parts of the models. This suggests they may be preferred when constructing a 3D model for more regional structures located at depths > 2 km. The dips interpreted from integrated use of geophysical models correlate reasonably well with previous geological interpretations made from field observations. But there are differences that might be due to the difference between the scales used in the modelling. These differences give us new information and insights thanks to the ability of geophysical models to resolve deeper information.

OUTLOOK

This study suggests that models from independent 3D inversions of the geophysical data contain valuable information to be used for imaging and classifying geological structures in 3D. The data sets used here have different sensitivities and, when inverted jointly, can produce models with even more reliable information. Joint inversion of MT and gravity data has become a common practice and can be tried on these datasets. The valuable detailed structural information found in the seismic reflection data can be applied in the inversion of magnetic field data as constraints or *a priori* information to estimate the geometry of the geological structures more accurately. The detailed information resolved in the electrical resistivity models from the 2D inversion of considerably narrow-band VLF data matched the geological and borehole observations. This encourages us to suggest a detailed electromagnetic survey with higher frequencies, such as a controlled source and radio MT survey, to collect supplementary information to gain better understanding about the depth and lateral extent of the low-resistivity mineralized zones close to Vittangi village. The cause of a deep and extremely low-resistivity, low-density and low-susceptibility zone in the middle of section 3 is unknown and should be the subject of more scientific research.

ACKNOWLEDGEMENTS

Dr. Maxim Smirnov of Olou University (currently at Luleå University of Technology) kindly provided us with existing MT stations close to the study area.

REFERENCES

Arora, K., V.M. Tiwari, B. Singh, D. C. Mishra, and I. Grevemeyer, 2012, Three dimensional lithospheric structure of the western continental margin of India constrained from gravity modelling: implication for tectonic evolution: Geophysical Journal International, 190, 131-150.

Bastani, M., I. Antal Lundin, A. Savvaidis, J. Kamm, and S. Wang, 2015, Audiomagnetotelluriska (AMT) mätningar i Kiruna- och Lannavara området, preliminära resultat: Sveriges geologiska undersökning SGU-rapport 2015:10, 16 p. (In Swedish).

Bergman, S., L. Kübler, and O. Martinsson, 2000, Regional geological and geophysical maps of northern Norrbotten County: Bedrock map (east of the Caledonian orogen): Sveriges geologiska undersökning, Ba 56:1.

Bergman, S., L. Kübler, and O. Martinsson, 2001, Description of regional geological and geophysical maps of northern Norrbotten County (east of the Caledonian orogen): Sveriges geologiska undersökning Ba 56, 110 p.

Bergman, S., M. B. Stephens, J. Andersson, B. Kathol, and T. Bergman, 2012, Bedrock map of Sweden, 1:1 000 000 scale. Sveriges geologiska undersökning K 423.

Cherevatova, M., M. Yu. Smirnov, A. G. Jones, L. B. Pedersen, and MaSca Working Group, 2015, Magnetotelluric array data analysis from north-west Fennoscandia: Tectonophysics, 653, 1-19.

England, R. W. and J. Ebbing, 2012, Crustal structure of central Norway and Sweden from integrated modelling of teleseismic receiver functions and the gravity anomaly: Geophysical Journal International, 191 (1), 1-11.

Eriksson, B. and U. Hallgren, 1975, Berggrundsgeologiska och flygmagnetiska kartbladen Vittangi NV, NO, SV, SO: Sveriges geologiska undersökning Af Nr 13-16. (In Swedish).

Gerdin, P., L. Johansson, and J. Magnusson, 1980, Luoheankorvenmaa–Pysäjärvi samman ställning av utförda prospekteringsarbeten: Sveriges geologiska undersökning Brap80057, 14 p. (In Swedish).

Hedin, P., A. Malehmir, D. Gee, C. Juhlin, and D. Dyrelius, 2014, 3D interpretation by integrating seismic and potential field data in the vicinity of the proposed COSC-1 drill site, central Swedish Caledonides: Geological Society of London, Special Publications, 390, 301-319

Juhojuntti, N., S. Olsson, S. Bergman, and I. Antal Lundin, 2014, Reflexionsseismiska mätningar vid Kiruna – preliminär tolkning: Sveriges geologiska undersökning SGU-rapport 2014:05, 26 p. (In Swedish).

Kamm, J., I. Antal Lundin, M. Bastani, M. Sadeghi, and L. B. Pedersen, 2015, Joint inversion of gravity, magnetic and petrophysical data - A case study from a gabbro intrusion in Boden, Sweden: Geophysics, 80(5), B131-B152.

Li, Y. and D. W. Oldenburg, 1998, 3D inversion of gravity data: Geophysics, 63, 109–119.

Lynch, E. P. and J. Jönberger, 2013, Summary report on the geological and geophysical characteristics of the Nunasvaara key area (29K Vittangi NO & SO): Sveriges geologiska undersökning, SGU-rapport 2013:11, 35 p.

Martinsson, O., 1993, Greenstone and porphyry hosted ore deposits in northern Norrbotten: *PIM/NUTEK* report # 1, 77 p.

Martinsson, O., 1997, Tectonic setting and metallogeny of the Kiruna greenstones: PhD thesis, Luleå University of Technology.

Martinsson, O., 1999, Berggrundskartan 30J Rensjön SO, skala 1:50 000: Sveriges geologiska undersökning Ai 133. (In Swedish).

Martinsson, O., 2011, Kiskamavaara: a shear zone hosted IOCG-style of Cu-Co-Au deposit in Northern Norrbotten, Sweden: Presented at the 11th Biennial SGA meeting.

Öhlander, B., T. Skiöld, S.-Å. Elming, BABEL Working Group, S. Claesson, and D.H. Nisca, 1993, Delineation and character of the Archaean-Proterozoic boundary in northern Sweden: Precambrian Research, 64, 67-84.

Pilkington, M., 1997, 3-D magnetic imaging using conjugate gradients: Geophysics, 62, 1132–1142.

Portniaguine, O. and M. S. Zhdanov, 2002, 3-D magnetic inversion with data compression and image focusing: Geophysics, 67, 1532-1541.

Siripunvaraporn, W. and G. Egbert, 2000, An efficient data-subspace inversion method for 2D magnetotelluric data: Geophysics, 65, 791–803.

Siripunvaraporn, W., G. Egbert, Y. Lenbury, and M. Uyeshima, 2005, Three dimensional magnetotelluric inversion: Data-space method: Physics of the Earth and Planetary Interiors, 150, 3–14.

Zhdanov, M.S., A. Gribenko, and G. Wilson, 2012, Generalized joint inversion of multimodal geophysical data using Gramian constraints: Geophysical Research Letters, 39, L09301, 1-7.